Lipid-Gramicidin Interactions: Dynamic Structure of the Boundary Lipid by 2D-ELDOR

Antonio J. Costa-Filho, Richard H. Crepeau, Petr P. Borbat, Mingtao Ge, and Jack H. Freed
Department of Chemistry and Chemical Biology and National Biomedical Center for Advanced ESR Technology, Cornell University, Ithaca, New York 14853-1301 USA

ABSTRACT The use of 2D-electron-electron double resonance (2D-ELDOR) for the characterization of the boundary lipid in membrane vesicles of DPPC and gramicidin A′ (GA) is reported. We show that 2D-ELDOR, with its enhanced spectral resolution to dynamic structure as compared with continuous-wave electron spin resonance, provides a reliable and useful way of studying lipid-protein interactions. The 2D-ELDOR spectra of the end-chain spin label 16-PC in DPPC/GA vesicles is composed of two components, which are assigned to the bulk lipids (with sharp auto peaks and crosspeaks) and to the boundary lipids (with broad auto peaks). Their distinction is clearest for higher temperatures and higher GA concentrations. The quantitative analysis of these spectra shows relatively faster motions and very low ordering for the end chain of the bulk lipids, whereas the boundary lipids show very high "*y*-ordering" and slower motions. The *y*-ordering represents a dynamic bending at the end of the boundary lipid acyl chain, which can then coat the GA molecules. These results are consistent with the previous studies by Ge and Freed (1999) using continuous-wave electron spin resonance, thereby supporting their model for GA aggregation and H_{II} phase formation for high GA concentrations. Improved instrumental and simulation methods have been employed.

INTRODUCTION

Lipid-protein interactions and ESR

Lipid-protein interactions have been a topic of major interest, and several different techniques, such as scanning calorimetry, electron spin resonance (ESR), nuclear magnetic resonance, x-ray diffraction, and others have been used to determine the molecular aspects of such interactions, and how they affect the properties of both reconstituted and biological membranes (Jost and Griffith, 1982; Watts and De Pont, 1986; Freed, 1987, 2000; Selinsky, 1992). It is clear that membranes consist of a protein-containing lipid bilayer, where the membrane proteins are located such that their hydrophobic regions penetrate the lipid membrane, thus fixing them to the bilayer. These proteins can serve as receptors on the cell surface, being responsible for several cell functions such as signal transduction (Holowka and Baird, 1996), and ion transport (Warren et al., 1974; Lee, 1998). Although much is known about the dynamic structure of lipids in membranes, the lipid-protein interface remains less clear.

Past studies have shown that the lipids in protein-containing membranes can be divided into two classes: bulk lipids, which are typically characterized as being in a fluid phase, and the boundary lipids, which are in close contact with the protein (Jost et al., 1973; Kang et al., 1979; Marsh and Watts, 1982).

ESR has been widely applied to investigations of membrane properties (Hubbell and McConnell, 1971; Berliner, 1976; Marsh, 1985; Freed, 1994, 2000), and has played an important role in identifying and characterizing the boundary lipid component in systems as diverse as cytochrome oxidase (Jost et al., 1973), rhodopsin (Watts et al., 1979), Na, K-transporting ATPase (Arora et al., 1999), and gramicidin A′ (GA) (Ge and Freed, 1993, 1999; Marsh, 1997). The latter is a well-known system for studies of lipid-protein interactions due to the commercial availability of GA, its prompt incorporation into lipid bilayers, and its simple structure. GA is a hydrophobic pentadecapeptide that, depending on its concentration in the membrane, can either form a dimer channel spanning the membrane, or else GA aggregates (Chapmann et al., 1977; Killian, 1992; Ge and Freed, 1999). At low concentrations of GA (GA:lipid $<$ 1:15), it has been found that GA has a dehydrating effect and exhibits hydrophobic mismatch (Fig. 1 *A*) (Ge and Freed, 1999). For GA concentrations greater than GA:lipid $=$ 1:15, it is believed that these effects cause the GA dimer channels to dissociate, followed by aggregation of the GA, which induces H_{II} phase formation (Killian and de Kruijff, 1985a,b, 1988; Van Echteld et al., 1982; Ge and Freed, 1999). Aggregation of this type is a crucial step for many biological processes occurring in biomembranes. (Schreiber et al., 1983; Kahn et al., 1978; Robertson et al., 1986; Holowka and Baird, 1996).

Nearly all of the ESR studies on membranes have employed conventional continuous-wave ESR (cw-ESR). Most of these studies relied on ''titration'' of the spectra of the bulk component to extract out the residual spectrum from boundary lipid, about which qualitative inferences could be

Submitted August 9, 2002, and accepted for publication December 23, 2002.

Address reprint requests to Prof. Jack H. Freed, Dept. of Chemistry and Chemical Biology, B52 Baker Laboratory, Cornell University, Ithaca, NY 14853. Tel.: 607-255-3647; Fax: 607-255-0595; E-mail: jhf@ccmr.cornell.edu.

Antonio J. Costa-Filho's present address is Biophysics Group, Instituto de Física de São Carlos, Universidade de São Paulo, C.P. 369, São Carlos 13560-970, Brazil.

© 2003 by the Biophysical Society

0006-3495/03/05/3364/15 $2.00

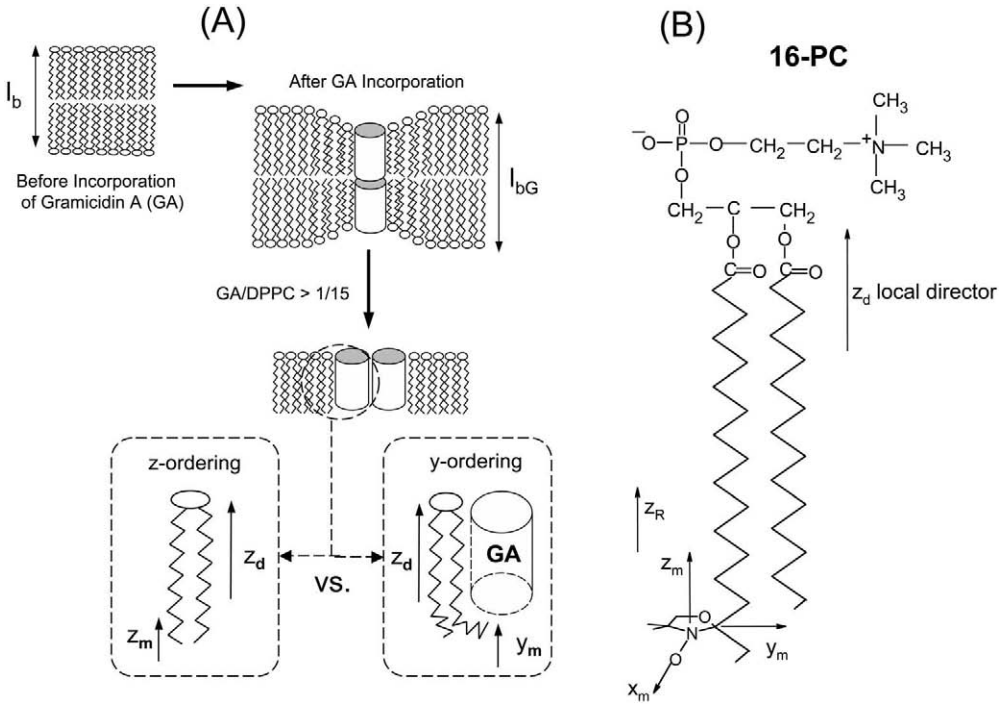

FIGURE 1 (*A*) Sketch of the effects of the presence of GA molecules in lipid bilayer at concentrations lower and higher than DPPC/GA = 15. (*B*) Molecular structure of the spin label 16-PC in its all-*trans* conformation (*z*-ordering).

made. However, since it was shown that the presence of peptide or protein in the membrane can significantly affect the dynamic structure of the bulk lipids (Ge and Freed, 1993, 1999; Ge et al., 1994; Patyal et al., 1997), it follows that such a titration procedure, which uses the spectrum from the pure lipid as a reference, may not be reliable. Thus one should deal directly with the protein-containing spectrum, and try to extract out information on the dynamic structure of bulk and boundary lipids, for example by modern methods of ESR spectral simulations (Schneider and Freed, 1989; Budil et al., 1996). Even when detailed simulations are carried out (Meirovitch et al., 1984; Ge and Freed, 1993, 1999), the complex ESR spectra from many biological studies can be misinterpreted due to their limited resolution. This low resolution results to a large extent from the fact that the observed spectrum is a superposition of spectra from microscopically ordered regions that, in turn, are macroscopically distributed over all orientations in vesicle dispersions. This is the so-called MOMD effect, for ''microscopic order'' with ''macroscopic disorder''. This spectral superposition is a major source of inhomogeneous broadening that masks the homogeneous broadening relating to molecular dynamics, leading to greater ambiguities in the fits of cw-ESR spectra, especially in the presence of two or more types of lipids. The use of macroscopically aligned samples can help, but Freed and coworkers (Ge et al., 1994; Ge and Freed, 1998) have pointed out that there are significant differences in details of dynamic structure for oriented samples as compared to vesicles, and this is true in particular for the effects of GA. Furthermore, for many biologically relevant systems, it may not be conveniently possible to prepare macroscopically aligned samples, whereas macroscopically disordered ''dispersion'' samples containing spin-labeled molecules may readily be prepared.

2D-ELDOR

More recently, 2D-FT-ESR techniques have been shown to have enhanced spectral resolution to ordering and dynamics compared to conventional cw-ESR for studying membrane vesicles (Crepeau et al., 1994; Lee et al., 1994). Patyal et al. (1997) obtained reliable ordering and dynamic parameters for the bulk lipid in the liquid crystalline phase of vesicles containing GA by means of 2D-electron-electron double resonance (2D-ELDOR). However, no evidence for the boundary lipid was observed in that study. It was postulated that this is due to the shorter T_2 values of the boundary lipid, due to slower motion and greater ordering that results in a faster decay of its ESR signal during the spectrometer dead time.

The 2D-ELDOR experiment is closely analogous to the 2D-exchange experiments of NMR, (Gorcester and Freed, 1988; Patyal et al., 1990; Gorcester et al., 1990; Crepeau et al., 1994; Lee et al., 1994). The 2D-ELDOR pulse sequence is illustrated in Fig. 2 *A*. It consists of three $\pi/2$ pulses. One collects the free induction decay (FID) along t_2 (after the spectrometer dead time, t_d) for fixed values of t_1, the preparation time and T_m, the mixing time. This process is repeated for different values of t_1 keeping T_m fixed. A double Fourier transform in t_1 and t_2 converts the signal, $S(t_1, t_2)$ into $\tilde{S}(f_1,f_2)$, which is a function of the two respective frequencies: f_1 and f_2, as shown in the contour plots of Fig. 3. Actually, one collects a ''hypercomplex'' signal, i.e., a signal that is complex, with a real absorptive

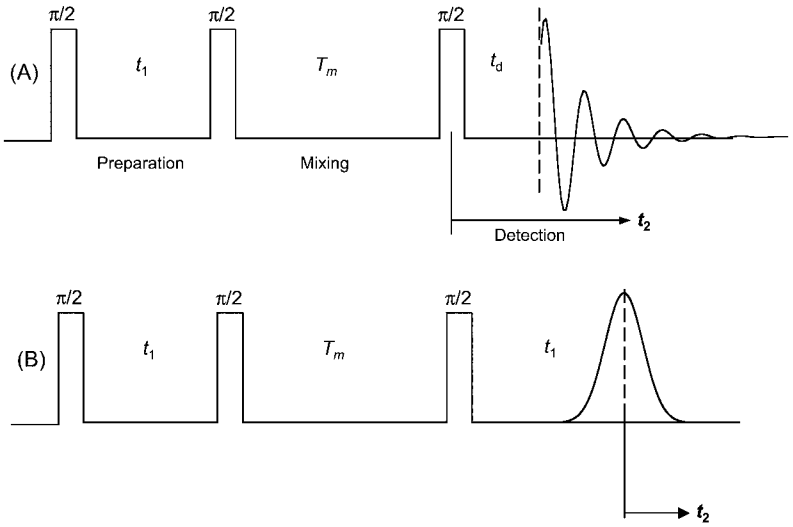

FIGURE 2 2D-ELDOR pulse sequence used for 2D-ESR experiments: (*A*) standard or COSY mode; (*B*) SECSY mode.

part and an imaginary dispersive part, with respect to each frequency in the 2D representation. This hypercomplex signal can be combined to give two ordinary complex signals that we call S_{c+} and S_{c-}. The former (the S_{c+} signal) is FIDlike, because it is not refocused by the last or ''read-out'' pulse, whereas the second (the S_{c-} signal) is echolike, because it is refocused by the last pulse. In the absence of inhomogeneous broadening (IB), the two are identical. In the presence of IB the S_{c+} and S_{c-} signals are quite different, with the S_{c-} spectra being substantially sharper due to the echolike cancellation of the IB, which does not occur for the S_{c+} spectra. In our past studies on membrane vesicles (Crepeau et al., 1994; Patyal et al., 1997) we have found that the S_{c+} signal is much more attenuated, due to its more rapid decay during t_d, because the IB is not refocused. Thus, we make use of the strong and better resolved S_{c-} signal, or more precisely its magnitude as in previous studies, which is the most convenient representation.

In Fig. 3, the so-called auto peaks are observed along the diagonal corresponding to $f_1 = f_2$. This diagonal corresponds closely to a conventional ESR spectrum (which, however is in the derivative mode unlike 2D-ELDOR) showing three hyperfine (hf) lines (most clearly seen in the spectra from pure DPPC at the higher temperatures). Conventional ESR spectra from these samples are shown in Fig. 4. Note that the high (low) field hf line in a conventional derivative ESR

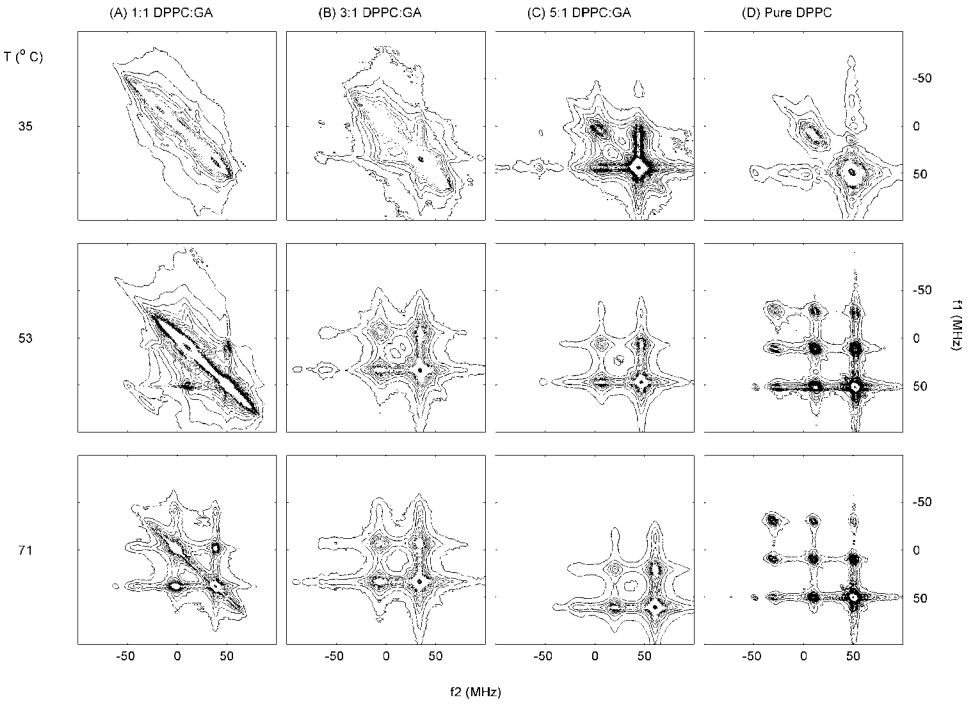

FIGURE 3 2D-ELDOR (17.3 GHz) contours for 16-PC at 35, 53, and 71°C, and mixing time, $T_m = 1600$ ns. (*A*) 1:1 DPPC:GA; (*B*) 3:1 DPPC:GA; (*C*) 5:1 DPPC:GA; (*D*) pure DPPC.

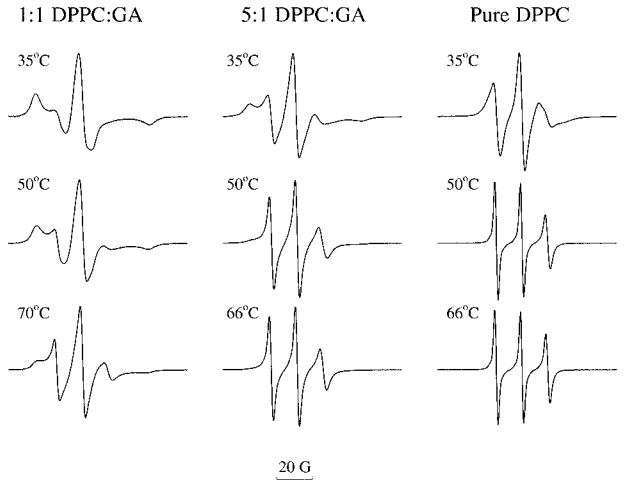

FIGURE 4 Derivative ESR spectra (9.3 GHz) for 16-PC at 35, 50, and 70 (or 66°)C for 1:1 DPPC:GA, 5:1 DPPC:GA, and pure DPPC.

spectrum becomes the low (high) frequency auto peak in the 2D-ELDOR spectrum. The peaks that are observed corresponding to $f_1 \neq f_2$ (again most clearly seen in the spectra from pure DPPC at the higher temperature) are known as the crosspeaks. These crosspeaks are a measure of magnetization transfer between hf lines by spin relaxation processes during T_m. The principal spin relaxation mechanisms are the intramolecular electron-nuclear dipolar interactions, which lead to nuclear spin flip transitions (with rate W_n) that report on the rate of rotational reorientation, and the Heisenberg exchange (HE) rate, ω_{HE}, which reports on the bimolecular collision rate of the spin-labeled molecules. The pattern of crosspeaks enables one to distinguish the contributions from each relaxation mechanism. In the present study, we used low enough concentrations to keep ω_{HE} small. The 2D-ELDOR experiments are done as a series of different T_m to observe how these crosspeaks ''grow-in'' relative to auto peaks, as a result of these cross-relaxation mechanisms. Such a series of 2D spectra versus T_m provides, in effect, a third dimension.

IB plays an important role in the case of MOMD spectra from membrane vesicles in 2D-ELDOR. It is possible to utilize the different shapes of the auto peaks and crosspeaks to distinguish the contribution to IB from proton super hyperfine (shf) interactions, which is the same for each hf line, and the MOMD effect, which varies for each hf line. As we noted, for the S_{c-} 2D-ELDOR spectra, there is a partial suppression of IB of the auto peaks due to their echolike properties. However, since the IB due to MOMD is different for the different hf lines, and the crosspeaks result from magnetization transfer between different hf lines, then the echolike cancellation is less effective for these peaks. Therefore, the crosspeak shapes, compared with the auto peak shapes, provide a sensitive measure of the MOMD inhomogeneity effects and hence the extent of ordering. In cases of high ordering, the effect of MOMD can be clearly discerned even in the shapes of the auto peaks (cf. Fig. 3 for the cases of lower temperature and higher GA concentration). Along the $f_1 = f_2$ diagonal, one observes the full IB, comparable to a cw-ESR experiment. However, in the perpendicular direction, the widths are reduced by the echolike cancellation effect discussed above.

There is a variant of the 2D-ELDOR experiment of Fig. 2 *A*, which leads to the homogeneous broadening (HB) being clearly displayed along one spectral dimension (i.e., f_1), whereas the auto peaks and their IB appear along the other (i.e., f_2) spectral dimension. This may be achieved by the modification shown in Fig. 2 *B*, which emphasizes the detection of the echo decay. The case of Fig. 2 *A* is referred to as the COSY (for correlation spectroscopy) mode, whereas that of Fig. 2 *B* as the SECSY mode (for spin-echo correlation spectroscopy). It has been shown theoretically (Gamliel and Freed, 1990; Lee et al., 1994) that: 1), an experiment performed in the COSY mode may be translated into the SECSY mode simply by letting t_2 in the former be replaced by $t_1 + t_2$ (thus redefining t_2) in the processing of the data, as is suggested by Fig. 2, and then performing a Fourier transform (FT) with respect to t_1 and the redefined t_2. Also 2), the homogeneous linewidths are indeed displayed along f_1. This clear separation of IB and HB of the auto peaks is extremely valuable in analyzing 2D-ELDOR spectra for cases where crosspeak development is very weak. We will have occasion to benefit from this SECSY mode in the present study.

These features for distinguishing between HB and IB as well as the development of crosspeaks are clearly absent in the cw-ESR spectra of Fig. 4. They will enable us, in the present study, to more reliably distinguish the dynamic structure of the boundary versus the bulk lipids.

Given the subtle interplay of various relaxation processes on the crosspeak intensities and the homogeneous linewidths, and of the various sources of inhomogeneous broadening on the auto- and crosspeaks, we find that the most effective way of extracting relevant relaxation and ordering data from 2D-ELDOR spectra is to perform nonlinear least-squares (NLLS) fitting of the 2D spectral simulations to the experimental spectra. The detailed theory and fitting are described elsewhere (Lee et al., 1994; Budil et al., 1996). We simultaneously fit the full 3D data set, (i.e., the set of 2D spectra obtained for different T_m).

In the present study, improved instrumental conditions (Borbat et al., 1997), such as dead times, reduced by about a factor of 2 to be as short as 25 ns, as well as improved signal-to-noise achievable at the higher frequency of 17.3 GHz (Patyal et al., 1997, used 9.2 GHz), have made it possible to apply 2D-ELDOR for more definitive characterization of the boundary lipid in DPPC/GA vesicles. For example, the broad spectrum from the boundary lipid is clearly seen superimposed on the sharper spectrum from the bulk lipid (cf. Fig. 3 for high GA concentration and high temperature). The two-component spectra of the spin label 16-PC in these vesicles

are then analyzed by the NLLS fitting procedure to obtain relevant ordering and dynamic parameters. This analysis, however, required that we generalize the NLLS 2D-ELDOR software of Budil et al. (1996) to include the capability for multiple spectral components in the usual 2D-ELDOR S_{c-} mode as well as in the SECSY mode.

Objective: dynamic structure of boundary lipid

The main objective of this paper is to clarify the recent study by Ge and Freed (GF) (1999) using cw-ESR on how the GA induces changes in the lipid phase structure, with the greatest attention to the role of the boundary lipid on the aggregation of GA. GF noted the ambiguity in interpreting the cw-ESR results, and they recommended 2D-ELDOR experiments to further clarify the dynamic structure of the boundary lipids. Their cw-ESR results had indicated ''that there is a dynamic bending at the end of the acyl chain of the boundary lipid'', which is associated with GA aggregates, and they interpreted this in terms of ''both the dehydration effect of GA (on the lipid bilayers) and the hydrophobic mismatch between GA and DPPC molecules.'' By hydrophobic mismatch, one means that the hydrophobic length of the GA channel is shorter than the thickness of the acyl chain region (cf. Fig. 1 *A*). Also, it has been observed that GA dehydrates the headgroup region of lipid bilayers by a preferential uptake of water by the GA channel (Killian and de Kruijff, 1985b). GF suggested that this must also dehydrate the lipid bilayers, resulting in their being compressed laterally and stretched longitudinally. Thus, the thickness of the acyl chain region increases, thereby enhancing the hydrophobic mismatch. It then follows that, whereas the bulk lipids in the bilayers are stretched and subject to tensions along the normal to the bilayer, the boundary lipids feel a compression resulting from their tendency to overcome the hydrophobic mismatch with the GA. Such opposing tendencies, GF suggest, can be relieved by a dissociation and vertical separation of the two GA molecules originally making up a dimer channel. Consistent with their observations, this occurs for GA/DPPC ratios >1:15. GF further argue that the dynamic bending of the acyl chains of the boundary lipid ''results in a negative curvature constraint at both leaflets of the bilayer, thus frustrating the bilayers in GA/DPPC dispersions, (which is) the driving force for the GA-induced H_{II} phase formation (Seddon, 1990; Gruner, 1985)'' at high GA/DPPC ratios >1:15. This gramicidin-induced H_{II} phase is characterized by a minimum of 1 gramicidin molecule per 7 lipid molecules, but much higher gramicidin concentrations can be accommodated (Killian and de Kruijff, 1988). Also, Cornell et al. (1988) have observed this nonlamellar phase up to 1:1 molar ratio. GF (1993) in their cw-ESR studies have shown that even at the molar ratio of 1:1, both boundary and bulk lipid components coexist.

Clearly the key ESR evidence for this model of the driving force for dissociation of GA channels, aggregation of GA, and formation of the H_{II} phase is provided in the dynamic structure of the boundary lipids, i.e., whether the ends of their acyl chains bend over from an all-*trans* configuration (cf. Fig. 1 *A*). We shall refer to the all-*trans* configuration as *z*-ordering, and to the bent configuration, *y*-ordering (cf. Fig. 1 *A*), for reasons discussed below.

It is a key objective of the present study to utilize the great sensitivity of 2D-ELDOR to dynamic structure to clarify these matters.

EXPERIMENTAL

Materials

Gramicidin A′ was obtained from Sigma Chemical (St. Louis, MO). The phospholipid 1,2-dipalmitoyl-sn-glycero-phosphatidylcholine (DPPC), and the spin label 1-palmitoyl-2-(16-doxyl stearoyl) phosphatidylcholine (16-PC) were purchased from Avanti Polar Lipids (Alabaster, AL.). All materials were used without further purification.

Preparation of model membranes

Stock solutions of the lipid DPPC and the spin label 16-PC in chloroform were mixed in a glass tube. The total weight of dried lipids was 2 mg, and the concentration of spins labels was 0.5 mol% of the lipids for all samples. Upon evaporation of the solvent by N_2 flow, the lipids formed a thin film on the wall of the tube. Then, the samples were evacuated with a mechanical pump overnight to remove trace amounts of the solvent. After the addition of 2 mL of 50 mM Tris (pH 7.0), 160 mM sodium chloride, and 0.1 mM EDTA, the lipids were scraped off the wall, and the solution was stirred for 1 min and kept in the dark at room temperature for at least 2 h for hydration. Samples were then pelleted using a desktop centrifuge, and transferred to a 1.5-mm i.d. capillary. Incorporation of GA into DPPC dispersions was achieved as described elsewhere (Patyal et al., 1997; Ge and Freed, 1999). Samples with molar ratios of GA/DPPC of 1/5, 1/3, and 1/1 were studied.

2D-ELDOR measurements

The experiments reported in this paper were performed on a home-built 2D-FT-ESR spectrometer as described in details elsewhere (Borbat et al., 1997). The 2D-ELDOR measurements were performed at 17.3 GHz (Ku band) and at different temperatures with the pulse sequence shown in Fig. 2 *A*. The 3.2-ns $\pi/2$ pulses provided practically uniform excitation of the nitroxide spectrum for the experimental conditions of this work.

The 2D-ELDOR spectra described below are obtained in the usual manner from a set of 1D data collections repeated 128 times with the interpulse separation, t_1, between the first two pulses being stepped out in 2.5 ns increments starting from an initial value of 40 ns (an initial delay of 35 ns is associated with the settling time of the phases shifter). In the 1D data collection, the FID signal was recorded after a t_d of ~25 ns (caused by the receiver overload) as a function of the time t_2 measured from the end of the third pulse in the sequence. The FID signal was collected in quadrature at a 200 MSPS rate with a dual-channel flash analog-to-digital converter with 10 kHz averaging capability (model TRACKH from DSP Technology (San Jose, CA)). This dwell time of 5 ns was effectively reduced to 1.25 ns by making four successive interleaves. For each channel, the four records were combined to yield a total of 256 data points in t_2. The quadrature FID signals were combined as required by the 32-step phase cycle sequence described elsewhere (Patyal et al., 1997), to form the ''hypercomplex'' signal consisting of S_{c+} and S_{c-} complex components (Gamliel and Freed, 1990), of which the latter was used in the subsequent data analyses.

Thus the typical 2D-ELDOR data collection can be viewed as a 128 × 256 2D set of complex points. A complete 2D-ELDOR experiment using a 9.6 kHz repetition rate for signal averaging required a total acquisition time of ~25 min. The collection was repeated for a set of T_m. This ''3D'' data set was obtained for a set of temperatures in the range 25–71°C for each of the three sample compositions studied.

To obtain 2D spectra in the frequency domain, $\tilde{S}(f_1,f_2)$ the S_{c-} component of the 2D time-domain data set $S(t_1, t_2)$ was Fourier transformed versus t_1 and t_2. We have used the magnitude spectrum to avoid phase problems caused by the finite dead times and deviations from uniform coverage (Gorcester and Freed, 1988; Patyal et al., 1990). For data-fitting purposes, some of the S_{c-} 2D spectra were also transformed into the SECSY representation by means of the shear transformation ($t_2 \rightarrow t_2 + t_1$) as described by Lee et al. (1994).

Cw-ESR experiments were performed on the same samples for comparison purposes using a Bruker Instruments EMX ESR spectrometer at a frequency of 9.34 GHz (X-band).

Nonlinear least-squares simulations

The Fourier-transformed magnitude spectra were analyzed to obtain the ordering, and the rotational and translational motional parameters. The analysis consists of an NLLS fit of the data to theoretical models based on the Stochastic-Liouville theory for time domain ESR (Schneider and Freed, 1989; Lee et al., 1994; Budil et al., 1996). The new version of the NLLS program developed for this study allows for fitting multicomponent spectra, as is required for the spectra from 16-PC in the DPPC/GA samples. The NLLS fitting also provides error estimates to the ordering and motional parameters as described by Budil et al. (1996). However, we have found in our recent cw-ESR and 2D-ELDOR studies that more reliable (and larger) error estimates are obtained by restarting the fitting with different sets of seed values for the parameters and determining the range of final values of these parameters. We have utilized these larger error estimates in the present study.

The simulation routine in the program makes use of the following coordinate systems to characterize the rotational dynamics and orientational ordering of the spin label. The first axis system is the laboratory frame (x_L, y_L, z_L), with its z axis being defined as the static magnetic field direction. The second coordinate frame is the bilayer orienting potential frame (x_d, y_d, z_d), also called the local director frame, which has its z_d axis parallel to the local bilayer normal. The third reference frame is the molecular diffusion frame (x_R, y_R, z_R), with the z_R axis being the main molecular symmetry axis. This is also taken as the molecular ordering frame for convenience, as well as usually by simple symmetry considerations. The fourth reference system is the magnetic tensor frame (x_m, y_m, z_m), in which the **g** and **A** tensors are defined. The x_m axis points along the N–O bond, the z_m axis is parallel to the $2p_z$ axis of the nitrogen atom, and y_m is perpendicular to the others. These coordinate systems are shown in Fig. 1 *B* for the spin label, 16-PC in its all-*trans* configuration. There, it can be seen that in this configuration, 16-PC is a ''*z*-ordering'' label, because its z_m axis is parallel to the z_R axis. The rotational mobility is represented by a rotational diffusion tensor, which is diagonal in the (x_R, y_R, z_R) principal axis system with components R_x, R_y, R_z characterizing the motion of the acyl chain. R_x and R_y represent reorientation of the z_R axis, whereas R_z represents rotation about this axis. In the all-*trans* configuration, characteristic of the 16-PC in the bulk lipid phase, it is typically found that $R_x \approx R_y$, and the motion can be simplified in terms of axially symmetric diffusion (Patyal et al., 1997). Furthermore, for this case one typically finds that $R_z \gg R_x$ and the fitting becomes rather insensitive to R_z (Patyal et al., 1997). We find these features for the bulk lipid, but not the boundary lipid, in the present study.

The orienting potential in the lipid bilayer, $U(\Omega)$, is expressed as an expansion in generalized spherical harmonics,

$$-U(\Omega)/kT = c_0^2 D_{00}^2(\Omega) + c_2^2[D_{02}^2(\Omega) + D_{0-2}^2(\Omega)], \qquad (1)$$

where $\Omega = (\alpha,\beta,\gamma)$ are the Euler angles between the molecular frame of the rotational diffusion tensor and the local director frame. The c_0^2 and c_2^2 are dimensionless potential energy coefficients representing the strength and asymmetry of the potential, k is Boltzmann's constant, and T is the temperature.

The order parameter, S_0, is defined as

$$S_0 \equiv \langle D_{00}^2[\Omega(t)]\rangle = \int d\Omega \exp(-U/kT) D_{00}^2 / \int d\Omega \exp(-U/kT) \qquad (2)$$

and measures the angular extent of the rotational diffusion of the nitroxide moiety. Thus, a large value of S_0 indicates very restricted motion. Another order parameter, S_2, is defined in a similar way as $S_2 \equiv \langle D_{02}^2[\Omega(t)] + D_{0-2}^2[\Omega(t)]\rangle$ and represents the deviation from axial symmetry of the molecular alignment relative to the local director. The meaning of positive and negative order parameters is discussed below (see Results and Discussion). The order parameters are thus used to express the local (microscopic) ordering of lipid molecules in the macroscopically disordered membrane dispersions.

The structure of the lipid dispersion, where locally the lipid molecules are aligned along a preferential axis, but globally the lipid bilayer segments are oriented randomly, gives rise to the MOMD effect (Meirovitch et al., 1984; Budil et al., 1996). The fitting program also takes these effects into account during the simulation procedure by treating the final spectrum as a superposition of the spectra from all fragments (Patyal et al., 1997; Lee et al., 1994). We found that varying the ''diffusion tilt'' angle between z_R and z_m had only marginal effect on the spectral fits. (Patyal et al. (1997) had found a small preference for a 31° tilt angle for the bulk lipid, whereas Ge and Freed (1999) found a preference for zero tilt angle for both types of lipid in their cw study). Additional fitting parameters included a Gaussian inhomogeneous broadening (Δ_G), which essentially accounts for the broadening from proton superhyperfine interactions, as well as a Lorentzian homogeneous width contribution, T_{2e}^{-1}, representing additional broadening mechanisms (Crepeau et al., 1994).

The fitting of the spectra in the SECSY format was found to be more stable in terms of convergence than the ones performed with the data in the S_{c-} format. Therefore, the spectra in the SECSY format were simulated first, and the parameters thus obtained were used as starting values for the S_{c-} fits. To make sure that the global minimum was reached, and to avoid local minima, we started the SECSY simulations with several sets of seed values. The **A** and **g** tensors needed for the fits were previously determined by cw simulations of rigid limit spectra (Ge and Freed, 1993; Tanaka and Freed, 1985). Further details of the fitting are discussed below.

RESULTS

2D-ELDOR spectra: boundary versus bulk lipid

We show in Fig. 3 a series of contour plots of 2D-ELDOR S_{c-} spectra taken at 17.3 GHz from 16-PC in lipid dispersions containing molar ratios of 0:1, 5:1, 3:1, and 1:1 of DPPC:GA at three temperatures: 35, 53, and 71°C. Since differences in these spectra are enhanced as T_m increases, only the spectra corresponding to the longest $T_m = 1600$ ns are shown. When compared to the cw-ESR spectra obtained for these DPPC:GA mixtures containing 16-PC shown in Fig. 4 (see also Ge and Freed, 1993, 1999), one notes the more dramatic variation of the 2D-ELDOR features, which is characteristic of its greater sensitivity to dynamic structure (Patyal et al., 1997; Borbat et al., 2001). In general, the higher the temperature, and the lower the GA concentration, the more characteristic are the spectra in Figs. 3 and 4 of typical spectra

from fluid phases. These 2D-ELDOR spectra show sharp and clear patterns of auto- and crosspeaks (Crepeau et al., 1994; Patyal et al., 1997). The sharp peak 2D-ELDOR spectra are ascribed to the bulk lipids, which are in the liquid crystalline phase above 41°C and the gel phase below 41°C. The bulk lipids in the liquid crystalline phase are also seen to yield their well-known sharp 3 hf line pattern in the cw-ESR spectra of Fig. 4. The gel phase spectra show broader lines in the 2D-ELDOR (as well as the cw-ESR) due to increased ordering and slower motions, but they are still characterized by the presence of a pattern of auto- and crosspeaks.

There is a second, very broad feature in the 2D-ELDOR spectra along the auto peak diagonal that becomes more prominent at higher GA concentrations and lower temperatures, as seen in Fig. 3. It is a dominant feature in the spectra from 1:1 DPPC:GA. We ascribe this broad 2D spectrum to that of the boundary lipid, whose concentration clearly must increase with concentration of GA. This broad boundary lipid spectral component is also prominent in the 3:1 DPPC:GA 2D spectrum at 35°C. Careful examination of the 3:1 DPPC:GA spectrum at 53°C and the 5:1 spectrum at 35°C also shows the presence of the broad boundary lipid component, although it is weaker. To illustrate this, we show an enhanced contour for this latter case in Fig. 5, which also includes the equivalently enhanced contour from pure DPPC vesicles at this temperature. The characteristic broad boundary lipid component is evident along the diagonal for the 5:1 spectrum. Such features could not be discerned in the study of Patyal et al. (1997) because of longer spectrometer dead times. The cw-ESR spectra in Fig. 4 also clearly show the two-component spectra for 1:1 DPPC:GA at 50° and 70°C, which is in agreement with the previous results of Ge and Freed (1993) at 45°C. For 5:1 DPPC:GA, the broader boundary lipid component is only weakly discerned at 50°C in Fig. 4 but is more prominent at 35°C in agreement with past cw-ESR studies (Ge and Freed, 1993, 1999), and with the present 2D-ELDOR results.

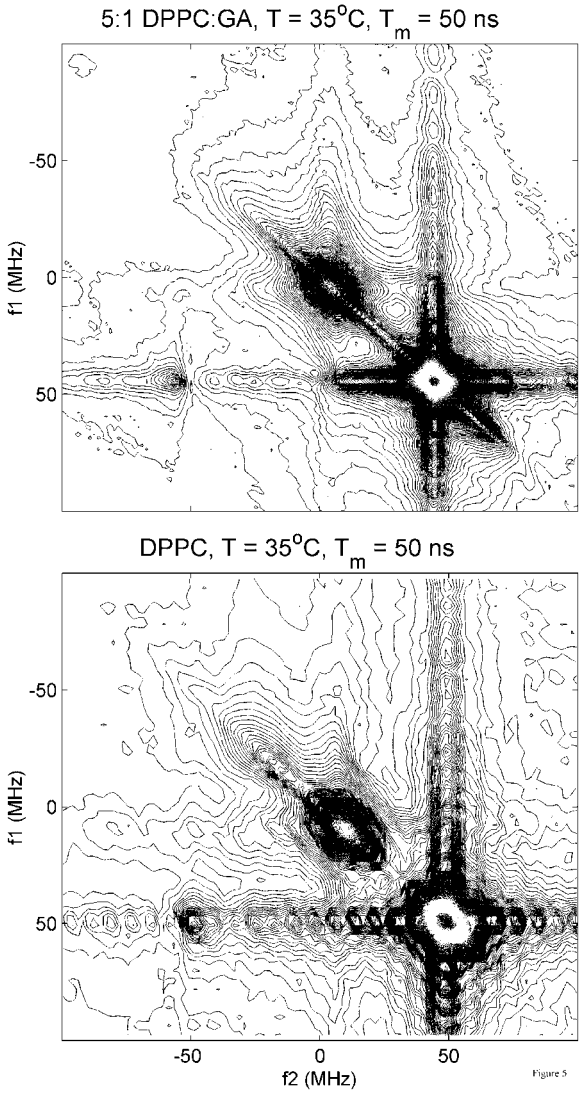

FIGURE 5 Enhanced 2D-ELDOR contours for 16-PC in 5:1 DPPC:GA at 35°C (*upper*) and in pure DPPC (*lower*) for $T_m = 50$ ns.

As in the previous ESR studies of Ge and Freed (1993, 1999) we interpret these two components at high GA to DPPC ratio as resulting from bulk and boundary lipids. This is also consistent with the previous studies of Killian et al. (1987), Killian and Kruijff (1988), and Cornell et al. (1988). The work of Killian and co-workers has shown that at high overall GA to DPPC ratio, there is a quantitative phase separation between a lamellar phase with a GA/lipid ratio of 1:15 and a hexagonal H_{II} phase, in which a minimum of one GA per seven lipid molecules is present, but much higher GA concentrations can be accommodated with GA molecules aggregated in clusters and oriented with their long axis perpendicular to the aqueous channel of the H_{II} phase. Cornell et al. (1988) verified the existence of phase separation in GA:DPPC (overall ratio 1:2 and 1:1) in which the GA-rich phase forms aggregates. Our results and these previous results taken together would seem to imply that at 1:1 DPPC:GA, the H_{II} phase with GA-enriched aggregates and a lamellar phase with a DPPC:GA ratio of ~15:1 are in coexistence. As will be shown below, the dynamic structure of the bulk lipids is quite similar to that found at somewhat higher ratio of DPPC:GA (i.e., 5:1), further supporting the existence of a lamellar phase. The boundary lipid component seen in both the 2D-ELDOR and the cw-ESR spectra of Figs. 3 and 4 is most likely primarily from the lipids in the H_{II} phase, where the very high GA concentration would guarantee that the lipids present are all in direct contact with GA molecules. On the other hand, we might expect that boundary lipids in the lamellar phase may have quite similar properties, as could be expected from the fact that each 16-PC molecule is directly interacting with an identical GA molecule in each phase. Ge and Freed (1999) found by cw-ESR some reduction of boundary lipid fraction with increased temperature (over the range 30–45°C) consistent with our observa-

tions. This suggests there is an increase in the lamellar phase fraction in coexistence with the GA-rich phase with increase in temperature.

The particular 2D-ELDOR spectrum that most clearly distinguishes the sharp pattern of auto- and crosspeaks from the bulk lipid versus the broad component from the boundary lipid is the 1:1 DPPC:GA ratio at 71°C. We therefore primarily focused on the set of spectra, as a function of T_m, obtained under these conditions for our detailed quantitative analysis. We also included the spectra from 53°C at this concentration for purposes of comparison. The 2D S_{c-} spectra as a function of T_m are shown in Fig. 6 for 71°C and Fig. 7 for 53°C.

To summarize our qualitative observations, 2D-ELDOR performed with very short dead times and pulses as short as 3 ns enables us to observe and distinguish the components from bulk lipid and boundary lipid. The latter yields a 2D-ELDOR spectrum with very broad auto peaks and no development of crosspeaks, whereas the bulk lipid spectrum is much sharper with substantial crosspeaks.

Spectral simulations and least-squares fitting

The simulation and fitting procedures utilized in this work have two new features as compared to previous studies (Crepeau et al., 1994; Patyal et al., 1997): 1), multicomponent 2D-ELDOR spectra were fit by means of NLLS; and 2), the experimental results in both the S_{c-} and SECSY modes were fit to better evaluate the quality of the fits.

Initial attempts at obtaining convergence in the simultaneous fitting of the two-component spectra in Fig. 6 proved difficult. However, we devised a successful three-step scheme to overcome this challenge. We first fit the bulk lipid component in the spectra using as seed values the parameters obtained by Patyal et al. (1997) for 16-PC in 5:1 DPPC:GA samples at 70°C. In this case, the usual fitting procedure with an axially symmetric rotational diffusion tensor was used, and the convergence to a reasonable fit was straightforward. Once this was achieved, these parameters for the bulk lipid component were kept fixed, and we started the second step, that of fitting the boundary lipid, i.e., the broad component. The initial attempts to fit the broad spectrum in the S_{c-} format presented substantial convergence problems. The fitting of the ordering and dynamic properties of the boundary lipid proved to be much more challenging than the fitting of the sharper spectra from the bulk liquid-crystalline phase accomplished above (or even in the gel phase described by Patyal et al. (1997)). However, we successfully overcame this difficulty by the following two modifications. First, to allow for a likely more complex dynamic structure for the spin labels in the boundary lipid region, we used a fully asymmetric rotational diffusion tensor for the boundary component instead of an axially symmetric one. Second, we transformed the 2D-ELDOR spectra in the S_{c-} format to their corresponding SECSY format by means of the shear transformation noted above, (cf. Fig. 8). This did resolve the convergence problems, and the SECSY fits proved to be more reliable than the S_{c-} ones. Furthermore (as discussed below), the use of both modes proved useful to help to resolve ambiguity problems in the fitting. The success of the SECSY format is that it separates the homogeneous broadening, which is displayed along the f_1 axis, from the inhomogeneous lineshape along the f_2 axis.

In the third and last step, we allowed all fitting parameters for both bulk and boundary lipids to vary simultaneously to achieve a final fit to the SECSY spectra. We used as the initial seed values for this step the results of steps 1 and 2. In general, the results of step 3 were found to be close to those of steps 1 and 2. Once the SECSY spectra were successfully fit in this manner, we used the resulting parameters as seed values to fit the spectra in the S_{c-} format. At this stage there was no problem to achieve convergence of the S_{c-} spectra, although resultant parameters showed some differences from those obtained from the SECSY fits.

To seek a global minimization in the fitting, we restarted step 2 with different seed values for the difficult-to-fit boundary lipid component. (The easier step 1 fitting of the bulk lipid component benefited from the prior results of Patyal et al. (1997) as already noted.) When we started with a negative or small positive order parameter, S_0, convergence was good, and we repeatedly found essentially the same χ^2 minimum in fitting the spectrum. However, it was also possible to find a less robust χ^2 minimum by starting with large positive values of S_0. By less robust we mean that a smaller set of seed values led to this second minimum. But the χ^2 values are comparable, and visual inspection (including the absolute values of the residuals) also shows them to be of comparable quality. Fig. 8, *top half* and *bottom half*, show the best spectral fits and residuals alongside the SECSY mode spectra for negative and positive order of the boundary lipid, respectively. Fig. 6, *top half* and *bottom half*, show the best fits and residuals alongside the S_{c-} spectra for negative and positive order of the boundary lipid, respectively. The analysis of such spectra in both the S_{c-} and SECSY modes leads to the dynamic and ordering parameters for the two cases of negative and positive ordering for the boundary lipid, which are given in Table 1, *A* (71°C) and *B* (53°C). We found ~10–20% boundary lipid and 90–80% bulk lipid, depending upon the spectral mode used (the S_{c-} and SECSY modes lead to different effective dead times (Crepeau et al., 1994; Lee et al., 1994), which can affect the measurement of relative populations) and the temperature for this 1:1 GA:lipid concentration. This seems reasonable in light of the more nearly equal amounts of boundary and bulk lipid found by GF for the 1:5 mixture at 45°C.

The parameters in Table 1 indicate that the boundary lipid undergoes slower rotational motion and experiences much greater ordering than the bulk lipid, irrespective of whether

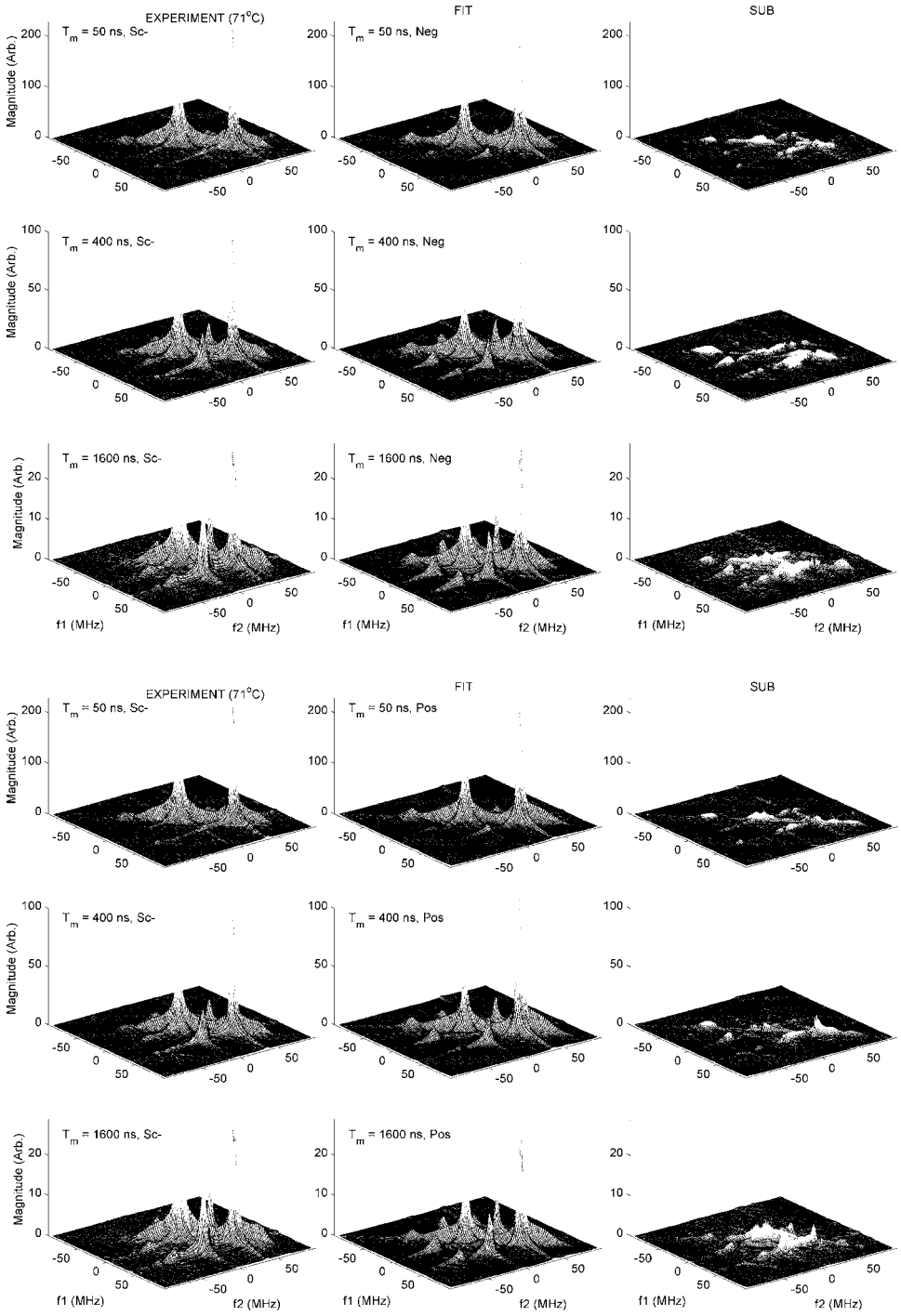

FIGURE 6 (*Top half*) Experimental (*left side*) and fitted (*middle*) 2D-ELDOR spectra in the S_{c-} format for assumed negative order of the label 16-PC in the boundary region in DPPC/GA vesicles as a function of mixing time T_m, at 71°C. The absolute value of the residual representing the difference between the experimental and fitted spectra is shown on the right in this and subsequent figures. (*Bottom half*) Experimental (*left side*), fitted (*middle*), and residual (*right side*) 2D-ELDOR spectra in the S_{c-} format for assumed positive order of the label 16-PC in DPPC/GA vesicles as a function of mixing time T_m, at 71°C.

we use the negative or positive ordering results. The low ordering and faster motion of the bulk lipid is consistent with previous studies (Patyal et al., 1997; Ge and Freed, 1999). In addition, the results for the bulk lipids are only mildly affected by positive versus negative ordering of the boundary lipid, or by the mode of representing the spectra (SECSY or S_{c-}). For the boundary lipid, the results for the rotational diffusion tensors are not greatly affected by these choices. Naturally, the values of S_0 and S_2 are considerably different for the negative versus positive ordering fits. There are also substantial differences in the ordering results in these two cases for SECSY versus S_{c-} fits, with the latter showing larger S_0 values. Since the SECSY spectra more clearly distinguish between homogeneous versus inhomogeneous broadening (or HB versus IB), we suspect that the S_{c-} spectral fits, in not as clearly providing this, lead to more imperfect results, also resulting in larger than expected (Gaussian) IB (cf. Table 1). (We observe in Table 1 that the

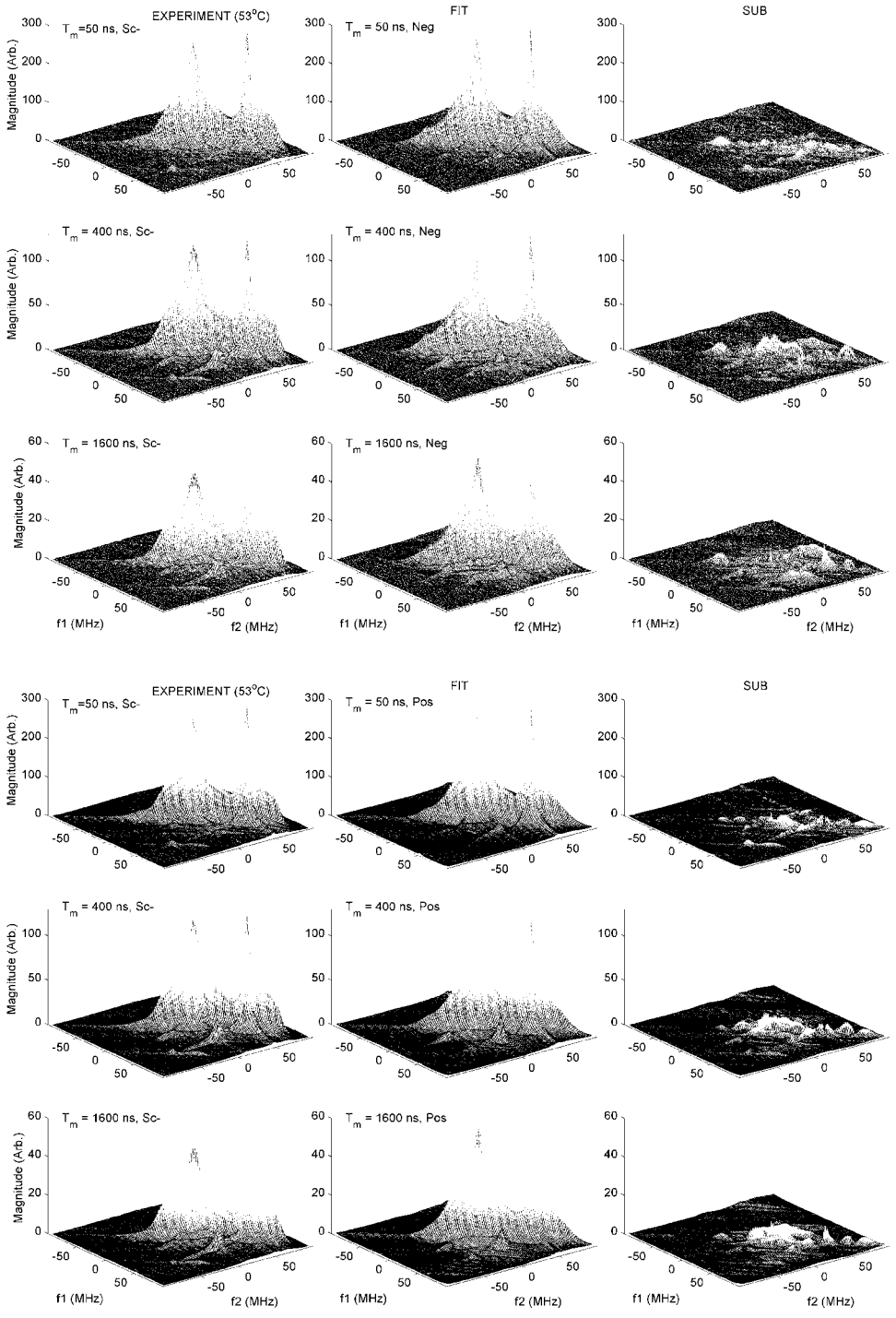

FIGURE 7 (*Top half*) Experimental (*left side*), fitted (*middle*), and residual (*right side*) 2D-ELDOR spectra in the S_{c-} format for assumed negative order of the label 16-PC in the boundary region in DPPC/GA vesicles as a function of mixing time T_m, at 53°C. (*Bottom half*) Experimental (*left side*), fitted (*middle*), and residual (*right side*) 2D-ELDOR spectra in the S_{c-} format for assumed positive order of the label 16-PC in the boundary region in DPPC/GA vesicles as a function of mixing time T_m, at 53°C.

IB is considerably greater for the boundary lipid as compared to the bulk lipid. The value for the latter is comparable to what was found by Patyal et al. (1997) in the liquid-crystalline phase as expected. The IB we find for the boundary lipid is even larger than the 2 G found by Patyal et al. for the bulk lipid in the gel phase (for DPPC:GA of 5:1). We suspect that this might point to greater heterogeneity in the local environments of the boundary lipid. Since the rotational diffusion tensors are comparable for the SECSY versus S_{c-} fits, the HB must be less for the case of the higher ordering obtained for the S_{c-} fits (Polnaszek and Freed, 1975; Lin and Freed, 1979). This reduced HB must be compensated by the increase in the values for the IB, as is found for the S_{c-} fits.)

It is useful to convert the order parameters S_0 and S_2 into their Cartesian representation S_{xx}, S_{yy}, S_{zz} in the magnetic

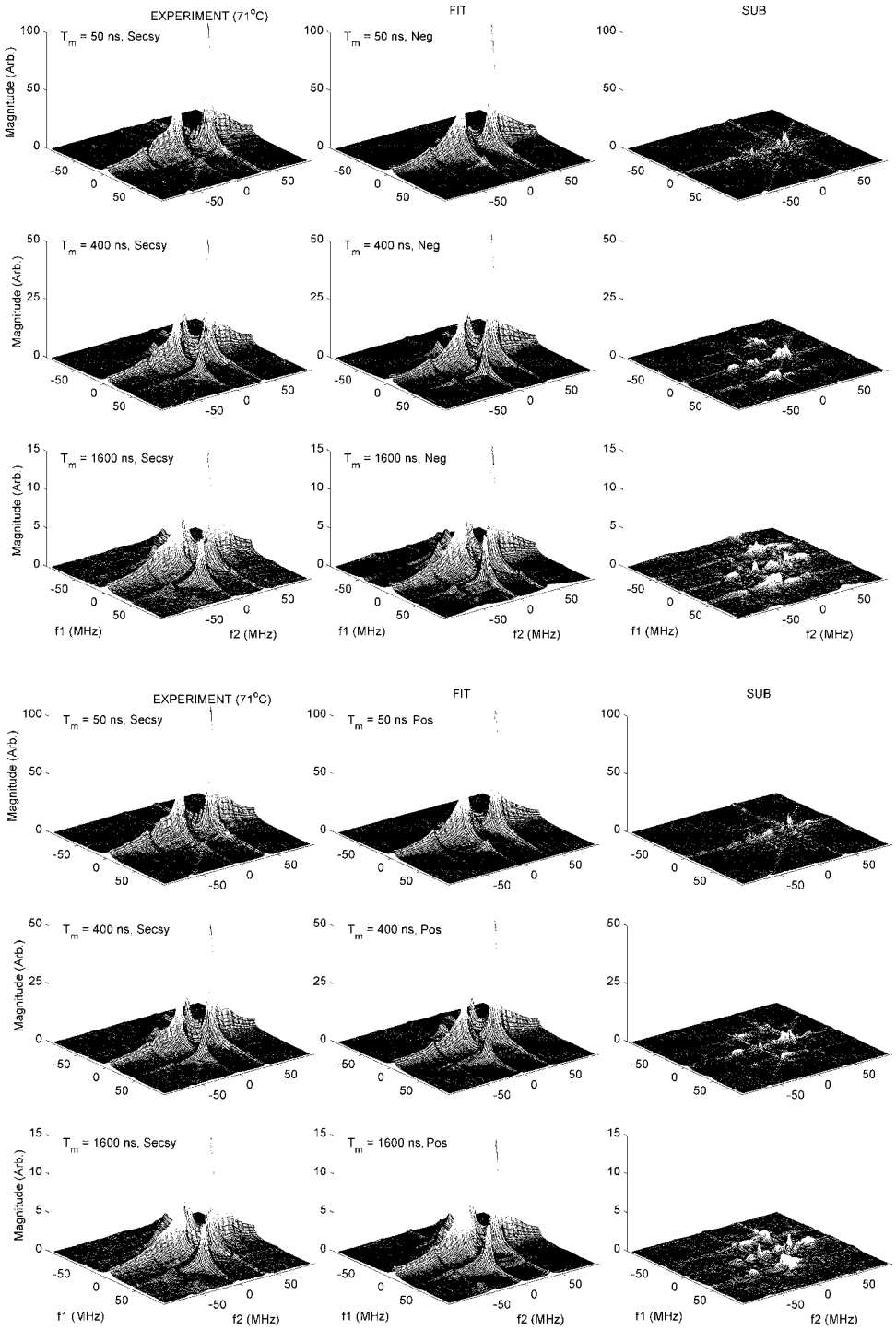

FIGURE 8 (*Top half*) Experimental (*left side*), fitted (*middle*), and residual (*right side*) 2D-ELDOR spectra in the SECSY format for assumed negative order of the label 16-PC in the boundary region in DPPC/GA vesicles as a function of mixing time T_m, at 71°C. (*Bottom half*) Experimental (*left side*), fitted (*middle*), and residual (*right side*) 2D-ELDOR spectra in the SECSY format for assumed positive order of the label 16-PC in DPPC/GA vesicles as a function of mixing time T_m, at 71°C.

tensor frame (Polnaszek and Freed, 1975; C. Zannoni, 1979) (we have dropped the subscript m for convenience). These are shown in Table 2. (Strictly, these order parameters refer to the diffusion or *R* frame, which can be tilted relative to the *m* frame. As noted in the Experimental section, the fitting was rather insensitive to this angle. We did, however, find that the bulk lipid fittings had a slight preference for tilt angles close to zero, and for the boundary lipid this slight preference ranged from ~15° to 30° for the different cases.) There it is seen that the case of negative ordering ($S_0 < 0$), corresponds to large and positive ordering about the magnetic y axis (cf. Fig. 1). That is, y_m strongly prefers to be parallel to the local director, z_d. The negative ordering of x_m and y_m implies they prefer to be normal to z_d. We refer to this as the y-ordering model. Note, that in this case our results show substantial asymmetry with respect to the

TABLE 1 Parameters obtained from nonlinear least-squares fitting of 2D-ELDOR spectra of 16-PC in vesicles of 1:1 DPPC:GA at 71°C and 53°C*†

Lipid	R_x (s^{-1})	R_y (s^{-1})	R_z (s^{-1})	S_0	S_2	T_2 (s)	Δ_g (Gauss)	Fraction
			(A) 71°C					
SECSY: *y*-ordering for the boundary lipid (negative order)								
Boundary‡	0.24×10^9	0.32×10^9	0.06×10^9	−0.22	−0.88	0.23×10^{-6}	2.9	0.90
Bulk§	0.62×10^9	0.62×10^9	6.2×10^9	0.04	0.09	0.32×10^{-6}	0.3	0.10
SECSY: *z*-ordering for the boundary lipid (positive order)								
Boundary¶	0.32×10^9	0.23×10^9	0.10×10^9	0.34	0.28	0.29×10^{-6}	2.8	0.86
Bulk‖	0.65×10^9	0.65×10^9	6.5×10^9	0.04	0.07	0.27×10^{-6}	0.3	0.14
S_{c-}: *y*-ordering for the boundary lipid (negative order)								
Boundary**	0.20×10^9	0.30×10^9	0.11×10^9	−0.43	−1.05	0.16×10^{-6}	3.8	0.78
Bulk††	0.73×10^9	0.73×10^9	7.3×10^9	0.06	−0.04	0.45×10^{-6}	0.4	0.22
S_{c-}: *z*-ordering for the boundary lipid (positive order)								
Boundary‡‡	0.37×10^9	0.23×10^9	0.12×10^9	0.73	0.12	0.22×10^{-6}	4.1	0.72
Bulk§§	0.67×10^9	0.67×10^9	6.7×10^9	0.06	−0.01	0.31×10^{-6}	0.4	0.28

Lipid	$R_\perp$ (R_x)	R_y	$R_\parallel$ (R_z)	S_0	S_2	Δ_g (Gauss)	Fraction
		(B) 53°C					
S_{c-}: *y*-ordering for the boundary lipid (negative order)							
Boundary¶¶	0.014×10^9	0.48×10^9	0.073×10^9	−0.45	−0.61	4.7	0.90
Bulk‖‖	0.12×10^9	–	1.2×10^9	0.20	−0.14	0.4	0.10
S_{c-}: *z*-ordering for the boundary lipid (positive order)							
Boundary***	0.034×10^9	0.63×10^9	0.12×10^9	0.77	−0.06	4.8	0.86
Bulk†††	0.15×10^9	–	1.5×10^9	0.17	−0.051	0.4	0.14

*Magnetic parameters for 16-PC: $A_{xx} = A_{yy} = 5.0$ G; $A_{zz} = 33.0$ G; $g_{xx} = 2.0089$; $g_{yy} = 2.0058$; $g_{zz} = 2.0021$ (Ge and Freed, 1993).
†The rotational diffusion and ordering tensor components are given in the principal axis frame of the rotational diffusion tensor, denoted by x_R, y_R, z_R, which is coincident with the magnetic tensor frame x_m, y_m, z_m (except perhaps for a small tilt angle between z_R and z_m, cf. text).
‡Estimated errors: R_x, R_y, R_z, 1%; S_0, S_2, 1%; $T_2 < 1\%$; Δ_g, 1%.
§Estimated errors: R_x, R_y, 1%; R_z, 70%; S_0, S_2, 8%; T_2, 1%; Δ_g, 10%.
¶Estimated errors: R_x, 7%; R_y, R_z, 12%; S_0, S_2, 10%; T_2, 3%; Δ_g, 2%.
‖Estimated errors: R_x, R_y, 1%; S_0, S_2, 15%; T_2, 10%; Δ_g, 4%; insensitive to R_z.
**Estimated errors: R_x, 15%; R_y, 5% ; R_z, 2%; S_0, S_2, 1%; T_2, 1%; Δ_g, 1%.
††Estimated errors: R_x, R_y, 4%; R_z, 50%; S_0, S_2, 5%; T_2, 1%; Δ_g, 1%.
‡‡Estimated errors: R_x, 25%; R_y, 5%; R_z, 3%; S_0, S_2, 2%; T_2, 20%; Δ_g, 1%.
§§Estimated errors: R_x, R_y, 2%; R_z, 5%; S_0, S_2, 5%; T_2, 1%; Δ_g, 2%.
¶¶Estimated errors: R_x, R_y, R_z, 1%; S_0, S_2, 1%; Δ_g, 1%.
‖‖Estimated errors: $R_\perp$, 1%; $R_\perp$, 10%; S_0, S_2, 5%; Δ_g, 1%.
***Estimated errors: R_x, R_y, R_z, 5%; S_0, S_2, 2%; Δ_g, 1%.
†††Estimated errors: $R_\perp$, 1%; $R_\parallel$, 9%; S_0, S_2, 1%; Δ_g, 1%.

degree of alignment of the y_m versus z_m axes in a direction normal to z_d.

We also fit the spectra for 1:1 DPPC:GA composition at 53°C, where the distinctions between boundary and bulk lipid component are less clear (cf. Fig. 7. We again used the above three-step procedure where the initial seed values were those obtained at 71°C in Table 1 *A* for both positive and negative S_0, with no further efforts to reseed and repeat the procedure. In this case, we just fit the S_{c-} spectra, and the results are in Table 1 *B*. We found ordering parameters for the boundary lipid that are quite similar to those obtained at 71°C, but the rotational diffusion tensor components show a sharply reduced R_x, slightly increased R_y, and a slightly reduced R_z. For the bulk lipid, the ordering parameters have increased substantially with the decrease in temperature, and the rotational diffusion tensor components have decreased significantly. Again, the fits for the *y*-ordering and *z*-ordering models lead to comparable χ^2 values, and visual inspection shows them to be comparable.

Although the χ^2 values do not distinguish between the two cases of *y*-ordering ($S_0 < 0$) versus *z*-ordering ($S_0 > 0$), we do note smaller estimated errors in the fitting parameters for *y*-ordering in Table 1. (Note also for *y*-ordering, the estimated errors for SECSY are smaller than for S_{c-}). We can apply another criterion that we have found useful in analyzing 2D-ESR spectra (Budil et al., 1996; Sastry et al., 1996). Basically it is to apply different methods of preparing or representing the spectra; then one observes which model fit is least sensitive to the mode of representing the experimental results. In the present case, this implies a comparison of the 71°C results for the SECSY and S_{c-} presentations. Using this criterion, we note that there is significantly less dramatic variation in the ordering tensors obtained for these two presentations in the case of the *y*-ordering versus the *z*-ordering model. (As noted above, there is not much variation in the rotational diffusion components). This criterion provides support for the *y*-ordering model, but this is clearly not conclusive. Additionally, as already noted, the *y*-order-

TABLE 2 Ordering tensor in Cartesian representation for the boundary lipids in DPPC/GA vesicles obtained as described in the text*

Mode—ordering	S_x	S_y	S_z	Tilt angle
71°C				
SECSY: *y*-ordering	−0.43	0.65	−0.22	22°
S_{c-}: *y*-ordering	−0.43	0.86	−0.43	31°
SECSY: *z*-ordering	0.00	−0.34	0.34	14°
S_{c-}: *z*-ordering	−0.29	−0.44	0.73	37°
53°C				
S_{c-}: *y*-ordering	−0.45	0.60	−0.15	29°
S_{c-}: *z*-ordering	−0.42	−0.35	0.77	23°

*These are given in the principal axis frame of the rotational diffusion tensor, denoted by x_R, y_R, z_R, which is coincident with the magnetic tensor, frame x_m, y_m, z_m (except perhaps for a small tilt angle between z_R and z_m, cf. text).

ing model proved to be considerably more robust in the fitting, since a wider range of seed values (including some for positive S_0) converged to it. This seems to lend further support to this model.

DISCUSSION

Patyal et al. (1997) showed that the greater resolution of 2D-ELDOR, especially as a function of T_m, allowed an unequivocal characterization of the dynamic structural changes of the bulk lipid as a result of addition of GA. In the present study using improved instrumentation with shorter dead times and greater sensitivity, it has been possible to provide an equivalent characterization of the boundary lipid. We do, in fact, observe the boundary lipid component in 5:1 DPPC:GA vesicle dispersions (cf. Fig. 5), unlike Patyal et al., as a result of this. However, in our analysis above we have utilized those spectra that most clearly distinguish the boundary and bulk lipid components for our extensive NLLS simulations and fitting.

Patyal et al. had concluded from the absence of a boundary lipid component in their 2D-ELDOR spectra that such a component ''is most likely one characterized by a reduced motional rate, but not so slow that it approaches the rigid limit, nor can it be one that is characterized primarily by substantially increased ordering.'' Using these results as guides, Ge and Freed (1999) interpreted their cw-ESR studies in terms of the *y*-ordering model for the boundary lipid as discussed above. Our present results are consistent with those found in these prior studies. For example, GF obtained for the boundary lipid in 5:1 DPPC:GA at 45°C (heating cycle): $S_0 = -0.40$, $S_2 = -0.28$, and $R_\perp = 0.02 \times 10^9\ s^{-1}$ (with $R_\parallel/R_\perp$ fixed at 10). Our results in 1:1 DPPC:GA at 53° (also a heating cycle) are $S_0 = -0.45$ and $S_2 = -0.61$ with $R_x = 0.014$, $R_y = 0.48$, and $R_z = 0.073$ in units of $10^9\ s^{-1}$. (Since cw-ESR does not provide a distinction between HB and IB, it is best to compare it with the mode of representing 2D-ELDOR, which does not provide the clearest distinction (Crepeau et al., 1994). Thus we use the S_{c-} results (as opposed to the SECSY results) for these comparisons.) Under the circumstances of somewhat different conditions (including differences in diffusion tilt angle) and the more limited resolution of the cw-ESR, this seems like satisfactory consistency. In fact, our S_0 and S_2 parameters are quite close to those obtained by GF for the 5:1 ratio in the temperature range of 30–40° (i.e., the gel phase, e.g., −0.44 and −0.62, respectively, for 40°C). This level of agreement from 2D-ELDOR and cw-ESR provides considerable support to the *y*-ordering model.

GF also found that there was a *z*-ordering fit to their data, which they rejected as less likely, because convergence to the *y*-ordering fit with different seed values was much more likely, as we have found in the present 2D-ELDOR study. Also some details of the cw spectrum were not as well fit. As we have already stated, our 2D-ELDOR results favor the *y*-ordering model, but purely on the basis of ESR studies we cannot rule out this second case, i.e., the *z*-ordering model. However, GF further argue that the *z*-ordering model with its substantial alignment is inconsistent with the disorder observed in the lipid chain due to high GA concentration using other techniques, whereas the *y*-ordering model corresponds to ''the end-chain segment, while undergoing rotational diffusion, is usually oriented such that its symmetry axis (the z_R axis) . . . is randomly distributed in the x_d-y_d local vesicle membrane plane. . . .'' We agree that these arguments lend further support to the *y*-ordering model.

One question that remains is why 2D-ELDOR, with its greater sensitivity to dynamic structure, does not in itself unequivocally distinguish between the *y*-ordering and *z*-ordering models. The problem here is most likely that of the limited orientational resolution of ESR at conventional frequencies, which, however, is greatly improved at higher frequencies (Freed, 2000; Borbat et al., 2001). We have tested this out by simulating the 2D-ELDOR spectra one would obtain for the two models at 95 GHz. Indeed, these simulations (not shown) show substantial differences, which would enable one to distinguish between them. Recent progress on high-power pulsed ESR at 95 GHz (Freed, 2000) may make it possible for such experiments in the future.

When we compare the present 2D-ELDOR results on the bulk lipid for 1:1 DPPC:GA with those of Patyal et al. (1997) for S_{c-} at 5:1 ratio, we find similar parameters: e.g., at 50°C their $S_0 = 0.19$, $S_2 = -0.07$ at 31° diffusion tilt versus the present $S_0 = 0.20$, $S_2 = -0.14$ (at 34° diffusion tilt and 53°C), and at 70°C their $S_0 = 0.084$, $S_2 = 0$ at 0° diffusion tilt versus the present $S_0 = 0.06$, $S_2 = -0.04$ (at −3° diffusion tilt and 71°C). Additionally, motional rates, reflected in $R_\perp$, are roughly comparable. Thus it would appear that there are no large changes in the properties of the bulk lipid phase, although this phase is necessarily decreased relative to the boundary lipid for the higher GA content. Thus the observation by Patyal et al. that the addition of substantial GA to DPPC reduces $R_\perp$ by a factor of 2–3 and increases S_0 a little is consistent with the observations of this study.

GF presented extensive evidence from their work and from previous studies that the lipids represented by the two

spectral components are most probably in different phase structures. For concentrations of GA:DPPC > 1:10, it is clear from past studies that an H_{II} phase is formed, as a result of the GA aggregation. It is also known that this phase can accommodate high gramicidin concentrations (Killian and de Kruijff, 1988). We expect, as did GF, that what we have been calling the boundary lipid refers mainly to those lipids in the H_{II} phase that contains aggregated GA. Thus the *y*-ordering model implied by our results shows that there is a dynamic bending near the end of the acyl chain of the boundary lipid. This supports GF's model in which this bending leads to a shrinkage of acyl chains, which arises from the hydrophobic mismatch between GA and the lipid, an effect that is more pronounced at high GA concentrations. The importance of this is that the hydrophobic mismatch is believed to provide a driving force for the formation of the H_{II} phase. Our 2D-ELDOR results thus provide strong evidence for the role of the boundary lipid that is consistent with the existence of a hydrophobic mismatch.

CONCLUSIONS

1. The considerable sensitivity of 2D-ELDOR to dynamic structure leads to distinctly different spectra for the two components present in DPPC/GA vesicles using the end-chain label 16-PC. These components are ascribed to lipids in distinctly different environments characterized as bulk and boundary lipids. The former have 2D spectra characteristic of lipids in a liquid crystalline phase, showing sharp peaks and crosspeak development as a function of mixing time, whereas the latter are much broader without significant development of crosspeaks.
2. The quantitative analysis of these 2D-ELDOR spectra shows that the boundary lipid is distinguished from the bulk lipid in its reduced motional rates characterized by a highly anisotropic rotational diffusion rate and much greater local ordering. This may be described as ''*y*-ordering'', which implies a bending of the end of the acyl chain so that it prefers to align parallel to the plane of the membrane bilayer, but is randomly aligned within that plane. The weak ''*z*-ordering'' of the bulk lipid implies weak alignment parallel to the normal to the membrane bilayer. These results are fully consistent with those obtained by Ge and Freed (1999) in their cw-ESR studies. Although there is another ''less robust'' spectral fit to the dynamic structure of the boundary lipid that corresponds to a large *z*-ordering, this is less consistent with the observation of end-chain disordering in studies using other physical methods.
3. These results are thus supportive of the model of Ge and Freed and other workers that ascribes an important role to hydrophobic mismatch between lipids and GA in the aggregation of GA and the formation of an H_{II} phase.
4. The sharp distinctions observed between boundary and bulk lipids in this study may be expected to serve as a basis for further studies of lipid-protein interactions in other systems of biological interest.

A.J.C.-F. thanks the Brazilian agency Conselho Nacional de Desenvolvimento Científico e Tecnológico for the financial support.

This work was supported by National Institutes of Health grants from the National Institute of General Medical Sciences and the National Center for Research Resources, and a grant from the National Science Foundation. Computations were performed at the Cornell Theory Center.

REFERENCES

Arora, A., M. Esmann, and D. Marsh. 1999. Microsecond motions of the lipids associated with trypsinized Na,K-ATPase membranes. Progressive saturation spin-label electron spin resonance studies. *Biochemistry*. 38: 10084–10091.

Berliner, L. J., editor. 1976. Spin Labeling: Theory and Applications. Academic Press, New York.

Borbat, P. P., A. J. Costa-Filho, K. A. Earle, J. Moscicki, and J. H. Freed. 2001. Electron spin resonance in studies of membranes and proteins. *Science*. 291:266–269.

Borbat, P. P., R. H. Crepeau, and J. H. Freed. 1997. Multifrequency two-dimensional Fourier transform ESR: an X/Ku-band spectrometer. *J. Magn. Reson*. 127:155–167.

Budil, D. E., S. Lee, S. Saxena, and J. H. Freed. 1996. Nonlinear-least squares analysis of slow-motion EPR spectra in one and two dimensions using a modified Levenberg-Marquardt algorithm. *J. Magn. Reson*. A120:155–189.

Chapmann, D., B. A. Cornell, A. W. Eliasz, and A. Perry. 1977. Interactions of helical polypeptide segments which span the hydrocarbon region of lipid bilayers. Study of gramicidin A lipid-water system. *J. Mol. Biol*. 113:517–538.

Cornell, B. A., L. E. Weir, and F. Separovic. 1988. The effect of gramicidin A on phospholipid bilayers. *Eur. Biophys. J*. 16:113–119.

Crepeau, R. H., S. Saxena, S. Lee, B. Patyal, and J. H. Freed. 1994. Studies of lipid membranes by two-dimensional Fourier transform ESR: enhancement of resolution to ordering and dynamics. *Biophys. J*. 66:1489–1504.

Freed, J. H. 1987. Molecular rotational dynamics in isotropic and oriented fluids studied by ESR. *In* Rotational Dynamics of Small and Macromolecules in Liquids. T. Dorfmuller and R. Pecora, editors. Springer-Verlag, Germany. 89–142.

Freed, J. H. 1994. Field gradient ESR and molecular diffusion in model membranes. *Annu. Rev. Biophys. Biomol. Struct*. 23:1–25.

Freed, J. H. 2000. New technologies in electron spin resonance. *Annu. Rev. Phys. Chem*. 51:655–689.

Gamliel, D., and J. H. Freed. 1990. Theory of two-dimensional ESR with nuclear modulation. *J. Magn. Reson*. 89:60–93.

Ge, M., D. E. Budil, and J. H. Freed. 1994. ESR studies of spin-labeled membranes aligned by isopotential spin-dry ultracentrifugation: lipid-protein interactions. *Biophys. J*. 67:2326–2344.

Ge, M., and J. H. Freed. 1993. An electron spin resonance study of interactions between gramicidin A′ and phosphatidylcholine bilayers. *Biophys. J*. 65:2106–2123.

Ge, M., and J. H. Freed. 1998. Polarity profiles in oriented and dispersed phosphatidylcholine bilayers are different: an electron spin resonance study. *Biophys. J*. 74:910–917.

Ge, M., and J. H. Freed. 1999. Electron-spin resonance study of aggregation of gramicidin in dipalmitoylphosphatidylcholine bilayers and hydrophobic mismatch. *Biophys. J*. 76:264–280.

Gorcester, J., and J. H. Freed. 1988. Two-dimensional Fourier transform ESR correlation spectroscopy. *J. Chem. Phys*. 88:4678–4693.

Gorcester, J., G. L. Millhauser, and J. H. Freed. 1990. Two-dimensional electron spin resonance. *In* Modern Pulsed and Continuous Wave Electron Spin Resonance. L. Kevan and M. Bowman, editors. Wiley, New York. 119–194.

Holowka, D., and B. Baird. 1996. Antigen-mediated IgE receptor aggregation and signaling: a window on cell surface structure and dynamics. *Annu. Rev. Biophys. Biomol. Struct.* 25:79–112.

Hubbell, W. L., and H. M. McConnell. 1971. Molecular motion in spin-labeled phospholipids and membranes. *J. Am. Chem. Soc.* 93:314–326.

Jost, P. C., O. H. Griffith, R. A. Capaldi, and G. A. Vanderkooi. 1973. Evidence for boundary lipid in membranes. *Proc. Natl. Acad. Sci. USA.* 70:480–484.

Jost, P. C., and O. H. Griffith, editors. 1982. Lipid-Protein Interactions, Vol. 2. John Wiley and Sons, New York.

Kahn, C. R., K. L. Baird, D. B. Jarrett, and J. S. Flier. 1978. Direct demonstration that receptor crosslinking or aggregation is important in insulin action. *Proc. Natl. Acad. Sci. USA.* 75:4209–4213.

Kang, S. Y., H. S. Gutowsky, J. C. Hsung, R. Jacobs, T. E. King, D. Rice, and E. Oldfield. 1979. Nuclear magnetic resonance investigations of the cytochrome oxidase-phospholipid interaction: A new model for boundary lipid. *Biochemistry.* 18:3257–3267.

Killian, J. A. 1992. Gramicidin and gramicidin-lipid interactions. *Biochim. Biophys. Acta.* 1113:391–425.

Killian, J. A., and B. de Kruijff. 1985a. Thermodynamic, motional, and structural aspects of gramicidin-induced hexagonal H_{II} phase formation in phosphatidylethanolamine. *Biochemistry.* 24:7881–7890.

Killian, J. A., and B. de Kruijff. 1985b. Importance of hydration for gramicidin-induced hexagonal H_{II} phase formation in doeylphosphatidylcholine model membranes. *Biochemistry.* 24:7890–7898.

Killian, J. A., and B. de Kruijff. 1988. Proposed mechanism for H_{II} phase induction by gramicidin in model membranes and its relation to channel formation. *Biophys. J.* 53:111–117.

Killian, J. A., K. N. J. Burger, and B. de Kruijff. 1987. Phase separation and hexagonal H_{II} phase formation by gramicidin A,B,C in dioleoylphosphatidyl choline model membranes. A study on the role of the tryptophan residues. *Biochem. Biophys. Acta.* 897:269–284.

Lee, A. G. 1998. How lipids interact with an intrinsic membrane protein: the case of the calcium pump. *Biochim. Biophys. Acta.* 1376:381–390.

Lee, S., D. E. Budil, and J. H. Freed. 1994. Theory of two-dimensional Fourier transform ESR for ordered and viscous fluids. *J. Chem. Phys.* 99:7098–7107.

Lin, W. J., and J. H. Freed. 1979. ESR studies of anisotropic ordering, spin relaxation, and slow tumbling in liquid crystalline solvents III: Smectics. *J. Phys. Chem.* 83:379–401.

Marsh, D. 1985. ESR probes for structure and dynamics of membranes. *In* Spectroscopy and Dynamics of Molecular and Biological Systems. P. M. Bayley and R. E. Dale, editors. Academic Press, London. 209–238.

Marsh, D. 1997. Magnetic resonance of lipids and proteins in membranes. *Curr. Opin. Colloid Interface Sci.* 2:4–14.

Marsh, D., and A. Watts. 1982. Spin labeling and lipid-protein interactions in membranes. *In* Lipid-Protein Interactions. P. C. Jost and O. H. Griffith, editors. John Wiley & Sons, New York. 53–126.

Meirovitch, E., A. Nayeem, and J. H. Freed. 1984. An analysis of protein-lipid interactions based on model simulations of ESR spectra. *J. Phys. Chem.* 88:3454–3465.

Patyal, B. R., R. H. Crepeau, D. Gamliel, and J. H. Freed. 1990. Two-dimensional Fourier transform ESR in the slow-motional and rigid limits: 2D-ELDOR. *Chem. Phys. Letts.* 175:453–460.

Patyal, B. R., R. H. Crepeau, and J. H. Freed. 1997. Lipid-gramicidin interactions using two-dimensional Fourier-transform electron spin resonance. *Biophys. J.* 73:2201–2220.

Polnaszek, C. F., and J. H. Freed. 1975. ESR studies of anisotropic ordering, spin relaxation, and slow tumbling in liquid crystalline solvents. *J. Phys. Chem.* 79:2283–2306.

Robertson, D., D. Holowka, and B. Baird. 1986. Cross-linking of immunoglobulin E-receptor complexes induces their interaction with the cytoskeleton of rat basophilic leukemia cells. *J. Immunol.* 136:4565–4572.

Sastry, V. S. S., A. Polimeno, R. H. Crepeau, and J. H. Freed. 1996. Studies of spin relaxation and molecular dynamics in liquid crystals by two dimensional Fourier transform ESR: I. Cholestane in butoxy benzylidene-octylaniline and dynamic cage effects. *J. Chem. Phys.* 105:5753–5772.

Schneider, D. J., and J. H. Freed. 1989. Calculating slow motional magnetic resonance spectra: a user's guide. *In* Biological Magnetic Resonance, Vol. 8. L. J. Berliner and J. Reuben, editors. Plenum Publishing, New York. 1–76.

Schreiber, A. B., T. A. Libermann, I. Lax, Y. Yarden, and J. Schlessinger. 1983. Biological role of epidermal growth factor clustering. *J. Biol. Chem.* 258:846–853.

Selinsky, B. S. 1992. Protein-lipid interactions and membrane function. *In* The Structure of Biological Membranes. P. Yeagle, editor. CRC Press, Boca Raton, FL. 573–601.

Tanaka, H., and J. H. Freed. 1985. Electron spin resonance studies of lipid-gramicidin interactions utilizing oriented multibilayers. *J. Phys. Chem.* 89:350–360.

Van Echteld, C. J. A., B. de Kruijff, A. J. Verkleij, J. Leunissen-Bijvelt, and J. de Gier. 1982. Gramicidin induces the formation of non-bilayer structures in phosphatidylcholine dispersions in a fatty acid chain length dependent way. *Biochim. Biophys. Acta.* 692:126–138.

Warren, G. B., P. A. Toon, N. J. M. Birdsall, A. G. Lee, and J. C. Metcalfe. 1974. Reconstitution of a calcium-pump using defined membrane components. *Proc. Natl. Acad. Sci. USA.* 71:622–626.

Watts, A., and J. J. H. H. M. De Pont, editors. 1986. Progress in Protein-Lipid Interactions, Vols. 1, 2. Elsevier, Amsterdam.

Watts, A., I. D. Volotovski, and D. Marsh. 1979. Rhodopsin-lipid associations in bovine rod outer segment membranes. Identification of immobilized lipid by spin-labels. *Biochemistry.* 18:5006–5013.

Zannoni, C. 1979. Distribution functions and order parameters. *In* The Molecular Physics of Liquid Crystals. G. R. Luckhurst and G. W. Gray, editors. Academic Press, New York. 51–83.